Negative thermal Hall conductance in a two-dimer Shastry-Sutherland model with a π-flux Dirac triplon

Sun, Hao; Sengupta, Pinaki; Nam, Donguk; Yang, Bo

2021

Sun, H., Sengupta, P., Nam, D. & Yang, B. (2021). Negative thermal Hall conductance in a two-dimer Shastry-Sutherland model with a π-flux Dirac triplon. Physical Review B, 103, L140404-. https://dx.doi.org/10.1103/PhysRevB.103.L140404

https://hdl.handle.net/10356/148837

https://doi.org/10.1103/PhysRevB.103.L140404

Letter

Negative thermal Hall conductance in a two-dimer Shastry-Sutherland model with a π-flux Dirac triplon

Hao Sun [1,*] Pinaki Sengupta,[2,†] Donguk Nam,[1,‡] and Bo Yang[2,3,§]

[1]*School of Electrical and Electronic Engineering, Nanyang Technological University, 50 Nanyang Avenue, Singapore 639798, Singapore*

[2]*School of Physical and Mathematical Sciences, Nanyang Technological University, 21 Nanyang Link, Singapore 637371, Singapore*

[3]*Institute of High Performance Computing, A*STAR, Singapore 138632, Singapore*

(Received 19 January 2021; accepted 30 March 2021; published 12 April 2021)

We introduce an effective two-dimer tight-binding model for the family of Shastry-Sutherland models with geometrically tunable triplon excitations. The Rashba pseudospin-orbit coupling induced by the tilted external magnetic field leads to elementary excitations having nontrivial topological properties with π-Berry flux. The interplay between the in-plane and out-of-plane magnetic field thus allows us to effectively engineer the band structure in this bosonic system. In particular, the in-plane magnetic field gives rise to a Berry curvature hotspot near the bottom of the triplon band and at the same time significantly increases the critical magnetic field for the topological triplon band. We calculate explicitly the experimental signature of the thermal Hall effect (THE) of triplons in $SrCu_2(BO_3)_2$ and show pronounced and tunabled transport signals within the accessible parameter range, particularly with a change of sign of the thermal Hall conductance. The tilted magnetic field is also useful in reducing the bandwidth of the lowest triplon band. We show it can thus be a flexible theoretical and experimental platform for the correlated bosonic topological system.

DOI: 10.1103/PhysRevB.103.L140404

Introduction. The Shastry-Sutherland model (SSM) [1] is a paradigmatic Hamiltonian for studying the interplay between geometric frustration and strong interactions in quantum magnets. The canonical SSM consists of the $S = 1/2$ antiferromagnetic Heisenberg model on the geometrically frustrated Shastry-Sutherland (SS) lattice [Fig. 1(a)]. In the strongly frustrated regime, the ground state is comprised of singlet dimers on the short bonds highlighted by the translucent ellipses. Its realization in $SrCu_2(BO_3)_2$ enabled various experimental studies [2–7] revealing rich many-body physics. In $SrCu_2(BO_3)_2$ layers of strongly interacting $S = 1/2$ copper atoms are arranged on the SS lattice with the nearest-neighbor (NN) spin moments on Cu atoms forming the singlet dimers arranged in a frustrated geometry [4,5,8]. Both theoretical and experimental developments explored the possibility of exotic states including spin liquids, spin supersolids, and complex magnetic textures [9–14]. In $SrCu_2(BO_3)_2$, small but nonzero anisotropies from the Dzyaloshinskii-Moriya (DM) interactions [15–18] impart a topological character to the lowest magnetic excitations. Because of the gapped dimer-singlet ground state and triplet elementary excitations [2,5–7], exotic phases of triplons can be obtained by varying the model parameters and employing field effects [7,16,19].

Bosonic analogs of topological phases have steadily gained interest over the past several years and have already been proposed with photons, phonons, and skyrmionic textures [20–23]. Recently, using a single dimer model, it was proposed that triplon excitations exhibit a topological phase transition in $SrCu_2(BO_3)_2$ in a weak magnetic field [7,16]. The out-of-plane magnetic field opens up a nontrivial band gap at the threefold degenerate Dirac point, giving rise to nonzero thermal Hall signals that can be, in principle, experimentally verified with transport measurements [16]. Since they are bosonic quasiparticles, triplon bands are normally populated by either thermally excited or magnetic field driven triplons. However, the bands retain their topological character only below a critical field and thermal excitations populate higher bands as well. These two factors could strongly suppress the strength of the THE in experiments. Moreover, at the theoretical level, the single-dimer model does not fully describe the nature of triplon excitations. Thus it is necessary to extend the tunable parameter space and the degrees of freedom (DOF) to uncover more interesting physics. The pseudospin DOF from the nonequivalent dimers can also have nontrivial physical consequences by coupling to the external magnetic field [24], and this is relatively unexplored in the literature.

In this Letter, we construct a two-dimer model for the frustrated Shastry-Sutherland model with the sublattice pseudospin DOF that couples to a tilted external magnetic field with both in-plane and out-of-plane components. Remarkably, the in-plane component gives rise to a new Dirac point between the lowest two triplon bands around the Brillouin zone (BZ) center. The elementary excitations—Dirac triplons (DT)—near the Dirac point have nontrivial topological properties with π-Berry flux [25]. With the out-of-plane magnetic field, the Dirac point is gapped with nonzero Berry curvature hot spot near the band minimum. We explicitly compute

*sunhao@ntu.edu.sg
†psengupta@ntu.edu.sg
‡dnam@ntu.edu.sg
§yang.bo@ntu.edu.sg

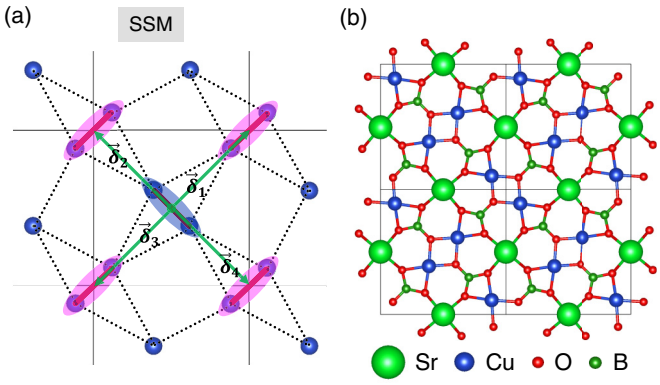

FIG. 1. Lattice structure of SSM and atomic structure of $SrCu_2(BO_3)_2$. (a) Lattice structure of Shastry-Sutherland model. (b) Top view of the monolayer $SrCu_2(BO_3)_2$. The magnetically active Cu^{2+} ions form a 2D arrangement of mutually orthogonal dimers.

the Hall response with different tilt angle and magnetic field strength, showing the pronounced tunable experimental signature for the THE, and provide theoretical evidence for the existence of external field induced DT. We point out there is a sign change of the thermal Hall signals as a function of the tilt angle, which is the typical feature of DT. The induced negative thermal Hall conductance reveals the flexible tunability of the thermal transport by the tilted magnetic field.

Microscopic model. At the microscopic level, the spin Hamiltonian with external magnetic field is given by [16]:

$$H = J\sum_{n.n.}\vec{S}_i\cdot\vec{S}_j + J'\sum_{n.n.n.}\vec{S}_i\cdot\vec{S}_j + \sum_{n.n.}\vec{D}_{ij}\cdot(\vec{S}_i\times\vec{S}_j) + \sum_{n.n.n.}\vec{D}'_{ij}\cdot(\vec{S}_i\times\vec{S}_j) + H_m, \tag{1}$$

where J is the isotropic intradimer exchange, $\vec{S}_j$ denotes the spin operator at site j, $\vec{D}_{ij}$ is the intradimer DM coupling, J' is the interdimer exchange with $J'/J \approx 0.63$, and $\vec{D}'_{ij}$ is the interdimer exchange. The dispersive triplon excitations come from the interactions between these spin dimers, and $H_m = -g\mu_B\sum_i \vec{h}\cdot\vec{S}_i$ is the Zeeman energy in the presence of an external magnetic field $\vec{h} = (h^x, h^y, h^z)$, with g as the g factor [7,16] and μ_B being the Bohr magneton [26]. Using the bond-operator language, and a mean field approximation, we transform the spin Hamiltonian in (1) into an effective tight-binding (TB) model: $H = H_{\text{site}} + H_{\text{hop}}$. H_{site} and H_{hop} are the onsite energy terms for the two dimers and hopping terms, respectively. The explicit form of the TB model is expressed as:

$$H_{\text{site}} = \sum_{\vec{r}} A^\dagger_{\vec{r}}\mathcal{N}A_{\vec{r}} + \sum_{\vec{r}'} B^\dagger_{\vec{r}'}\mathcal{N}B_{\vec{r}'},$$
$$H_{\text{hop}} = \sum_{\vec{r}}\sum_{n}^{4} B^\dagger_{\vec{r}+\vec{\delta}_n} M(\vec{\delta}_n)A_{\vec{r}} + \text{H.c.}, \tag{2}$$

where $A^\dagger_{\vec{r}} = (\tilde{t}^\dagger_{Ax,\vec{r}}, \tilde{t}^\dagger_{Ay,\vec{r}}, \tilde{t}^\dagger_{Az,\vec{r}})$ and $B^\dagger_{\vec{r}} = (\tilde{t}^\dagger_{Bx,\vec{r}}, \tilde{t}^\dagger_{By,\vec{r}}, \tilde{t}^\dagger_{Bz,\vec{r}})$ are the elementary excitations on individual dimers in the presence of DM interaction for the A and B dimers, respectively. The new triplon operators $\tilde{t}_{A,\vec{r}}(\tilde{t}_{B,\vec{r}})$ are formed by linear combinations of the standard triplon operators, in other words, a rotation in the local spin Hilbert space [26]. $\mathcal{N}$ is the diagonal onsite energy matrix. The coordinate $\vec{r}$ runs over the position of all unit cells, $\vec{\delta}_n$ is the nearest neighbor bond describing the two-dimer geometry as shown in Fig. 1(a), and M are the hopping matrices between the dimers, with the following forms:

$$M(\pm\vec{\delta}_1)(M(\pm\vec{\delta}_2)) = \frac{1}{2}\begin{pmatrix} 0 & -D'_\perp & 0(\mp\tilde{D}'_\parallel) \\ D'_\perp & 0 & \pm\tilde{D}'_\parallel(0) \\ 0(\pm\tilde{D}'_\parallel) & \mp\tilde{D}'_\parallel(0) & 0 \end{pmatrix}, \tag{3}$$

where $D'_\perp$ is the out-of-plane component of interdimer DM vector, and $\tilde{D}'_\parallel = D'_{\parallel,s} - \frac{DJ'}{2J}$ is the effective in-plane DM component. We set $J = 1$, $|\tilde{D}'_\parallel|/J = 0.03$, and $D'_\perp/J = -0.03$ in accordance with previous studies [7,16]. The external magnetic field part in Eq. (1) is given by:

$$H_m = \sum_{\beta,\gamma,\vec{r}} ig\epsilon_{\alpha\beta\gamma}h_\alpha\tilde{t}^\dagger_{A\beta,\vec{r}}\tilde{t}_{A\gamma,\vec{r}} + \sum_{\beta,\gamma,\vec{r}'} ig\epsilon_{\alpha\beta\gamma}h_\alpha\tilde{t}^\dagger_{B\beta,\vec{r}'}\tilde{t}_{B\gamma,\vec{r}'}. \tag{4}$$

This term modifies the onsite energy matrix $\mathcal{N}$ with additional off-diagonal elements:

$$\mathcal{N} = \begin{pmatrix} J & igh_z & -igh_y \\ -igh_z & J & igh_x \\ igh_y & -igh_x & J \end{pmatrix}, \tag{5}$$

which gives rise to exotic topological properties [7,16]. We fix the in-plane component of the magnetic field to be along the x direction, let $\vec{h} = (h_i, 0, h_z)$. To ensure the validity of the models in Eqs. (2) and (4), the external magnetic field $\vec{h}$ has to be of the same order as the DM strength which is small compared to the exchange strengths J and J'. Thus, only terms linear in $\tilde{D}'_\parallel$, $D'_\perp$, and $\vec{h}$ are kept when transforming the spin Hamiltonian in Eq. (1) to the effective TB model.

Triplon band and π-flux Dirac boson. Starting from Eq. (2), the Hamiltonian of triplon excitations with pseudospin in momentum space can be written in the following form:

$$\mathscr{H}(k) = \sigma_x\otimes m_x + \sigma_y\otimes m_y + \sigma_0\otimes\mathcal{N}, \tag{6}$$

where $m_x(k) = \frac{\mathscr{M}(k)+\mathscr{M}^\dagger(k)}{2}$, and $m_y(k) = i\frac{\mathscr{M}^\dagger(k)-\mathscr{M}(k)}{2}$. $\mathscr{M}(k) = \sum_n^4 e^{-i\vec{k}\cdot\vec{\delta}_n}M(\vec{\delta}_n)$ is a 3×3 traceless matrix that can be obtained from Eq. (3). σ_x and σ_y are Pauli matrices for the pseudospin, and σ_0 is 2×2 identity matrix. The calculated band structures with and without magnetic fields are shown in Fig. 2. The original lowest bands in Fig. 2(a) show a parabolic feature at the BZ center is twofold degenerate. When the out-of-plane magnetic field h_z is turned on, the degeneracy of the lowest triplon bands is lifted. The gap of the excitation spectrum near the zone center is proportional to h_z but vanishes at the points X and Y of the BZ edges. With only the in-plane magnetic fields, the lowest triplon bands undergo a Rashba-like splitting and form a gapless Dirac point at the Γ point as shown in Fig. 2(c). The anisotropic dispersion of the DT is also shown in Fig. 2(e), which depends on the orientation angle of the in-plane component. Thus the

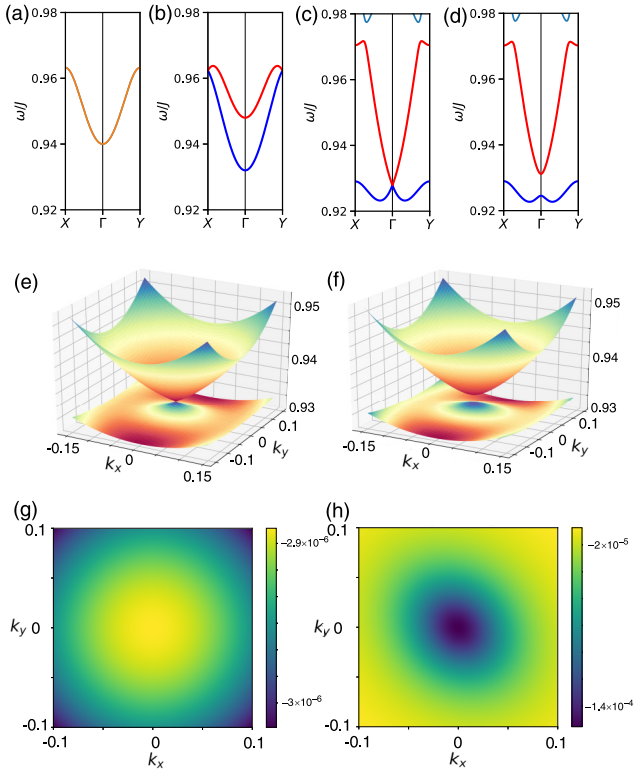

FIG. 2. Band structure of triplon excitations in SSM. (a) The lowest triplon bands are twofold degenerate at $\vec{h} = 0$. (b) The lowest triplon bands split into two subbands ($h_z/J = 0.008$). (c) The Dirac point of the lowest triplon bands at the Γ point ($h_i/J = 0.04$). (d) The Dirac point in (c) is gapped ($h_i/J = 0.04$, $h_z/J = 0.004$). The triplon band (e) near the Γ point at $h_i/J = 0.04$, and (f) near the Γ point at $h_i/J = 0.04$, $h_z/J = 0.004$. (g) The Berry curvature hot spot is nearly 0 ($h_z/J = 0.008$). (h) Large Berry curvature hot spot ($h_i/J = 0.04$, $h_z/J = 0.004$).

direction of the in-plane magnetic field can be a novel tuning knob for the transport of DT in this quantum magnet system.

We shall particularly focus on the case when the applied magnetic field has both nonzero in-plane and out-of-plane components. A finite h_z component lifts the twofold degeneracy of the Dirac point and opens up a gap in the dispersion at the Γ point as shown in Figs. 2(d) and 2(f). The nontrivial excitation gap results in a finite Berry curvature distribution around the zone center, which is near the bottom of the band as depicted in Fig. 2(h). In contrast, with only the out-of-plane magnetic field ($h_z/J = 0.008$), the Berry curvature is nearly zero at the band bottom [Fig. 2(g)].

To better understand the different roles of external magnetic components, we construct an effective low-energy theory of the lowest two bands near the Γ point from the original TB Hamiltonian as follows:

$$\mathscr{H}(k) = \frac{\hbar^2 k^2}{2\mu} + \alpha h_i(\sigma_x k_x + \eta\sigma_y k_y) + \beta h_z \sigma_z, \qquad (7)$$

where μ is the effective mass of parabolic triplon band. α, β are constants determined by $D'_\perp$ and $\tilde{D}'_\parallel$, and η is the coefficient for the anisotropic feature determined by the orientation of the in-plane component of the magnetic field. This

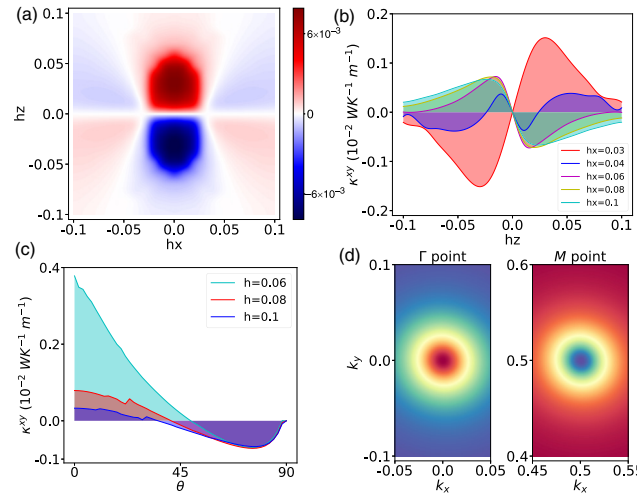

FIG. 3. The thermal Hall conductivity at 10 K. (a) The diagram of thermal Hall conductivity is a function of the magnetic field in the $h_x - h_z$ plane. (b) Thermal Hall conductivity along the h_z axis with different magnitudes of h_x component. (c) The angle-dependent Hall conductivity under a tilted magnetic field with different magnitudes. (d) The Berry curvature distributions of lowest triplon band.

effective model exactly reproduces the band structure near the Γ point and reveals the low energy behavior of the DT excitations. One can immediately identify it with the Rashba spin-orbit coupling (SOC) Hamiltonian in the fermionic systems [27,28]. In our case, h_i plays the role as the Rashba pseudospin-orbit coupling coefficient. The Dirac boson thus hosts a π flux from the Berry phase of a closed circle around the Dirac point: $\oint_C \langle\psi_k|i\partial_k|\psi_k\rangle dl = -\pi$. When DT anticrossing is gapped by the out-of-plane magnetic field h_z, this pointlike flux ϕ gives rise to the nonzero Berry curvature hot spot near the Γ point.

Bosonic thermal Hall effect. Given that the triplons are charge neutral, the THE allows us to probe the Berry curvature distribution in the bosonic systems. The thermal Hall conductivity κ^{xy} is given as follows [16,29]:

$$\kappa^{xy} = \frac{k_B^2 T}{(2\pi)^2 \hbar} \sum_n \int d^2k c_2(\rho_n) \Omega_n^{xy}(\vec{k}), \qquad (8)$$

where k_B is the Boltzmann constant, $\rho_n = \frac{1}{e^{\omega_n \beta} - 1}$ is the Bose-Einstein (BE) distribution function, $\beta = 1/(k_B T)$. $c_2(u)$ is the population function given by [29], and $\Omega_n^{xy}(k_x, k_y)$ is the Berry curvature. In the low-temperature limit, the dominant contribution to κ^{xy} comes from the lower bands, and the nonzero Berry curvature shown in Fig. 2(h) contributes to the thermal Hall conductivity. Thus, the change of the total thermal Hall conductivity provides a way to probe this π-flux boson in the triplon system. Figure 3(a) shows the calculated Hall conductivity in the $h_x - h_z$ parameter space. When $h_x > 0.04$, the Hall signal becomes negative at a positive h_z and positive at a negative h_z as shown clearly in Fig. 3(b). This interesting feature is due to the fact that the Berry curvature around the gapped DT point is always *opposite* those around the M point when the gap is opened by the h_z field. Since at the high-symmetric M point with its reciprocal position

(1/2,1/2) in BZ, the spin-1 Dirac cone is present, which also contributes to the THE as discussed in Ref. [16]. To illustrate this, we plot the schematic distributions of Berry curvature at the Γ and M point of the lowest triplon band at $h_x = 0.02$ and $h_z = 0.001$, which is shown in Fig. 3(d). The Berry curvature in the zone center (Γ point) shows a negative value, while a positive Berry curvature develops at the zone corner (M point).

The switch of the sign of the thermal Hall signal can be easily probed with an angle-dependent Hall measurement, which provides a concrete test for the existence of magnetic field-induced DT excitations. As shown in Fig. 3(c), the angle-dependent Hall signal with different magnetic field strength are plotted, where $\theta = \arctan(h_x/h_z)$ is the angle between tilted magnetic field $\vec{h}$ and the vertical z axis. The Hall signals are large at a very small h_x/h_z ratio and decay fast by increasing the ratio when $|\vec{h}| < 0.08$ (red line). When the threshold magnetic field strength $h_c \approx 1.4$ T is reached, the topological nature of the triplon bands is lost and the Hall signal κ^{xy} is suppressed. One can see the angle-dependent Hall signal (purple line with $|h| = 0.1$) is almost 0 at very small angle, where the band is trivial when $\theta < 30^\circ$. However, the situation is quite different when tuning the tilted angle larger than a critical value. The Hall signal shows a sign change and reaches a maximal negative value around the angle 77°. This sign change could be the solid evidence for the gapped π-flux DT induced by the in-plane magnetic field.

The thermal Hall signal in $SrCu_2(BO_3)_2$ is small due to the weak DM interaction, making the experimental detection more challenging. Increasing the orbital hybridization at the interface by proximity effect can potentially enhance the DM interactions. In order to maintain the validity of the effective TB model, we limit the enhancement of the DM parameter $\tilde{D}'_{\parallel}$ and $D'_{\perp}$ to be within three times the current values. Since the bandwidth is proportional to the DM interactions, the large DM interaction will give rise to a large triplon bandwidth. In addition, increasing of DM interactions will decrease the excitation gap, which gives rise to larger triplon populations. Both will lead to a more pronounced triplon thermal Hall signal.

Numerical calculations show the bandwidth without magnetic field is linear in the DM interactions as plotted in Fig. 4(a). The analytic solutions of bandwidth can also be found by solving the Hamiltonian $\mathscr{H}(k)$ at $k = 0$, which gives the bandwidth $\Delta\omega = 2D'_{\perp}$. We calculate the maximal negative Hall conductivity induced by gapped DT by searching the $h_x - h_z$ plane, which also shows the surprising linear behaviors with respect to the increasing of $D'_{\perp}(\tilde{D}'_{\parallel})$. One can roughly understand this linear relation from the change of the activation gap $\Delta E = J - 2D'_{\perp}$ between the singlet and triplet excitations. The total population is approximately $P_t = e^{-\Delta E/k_B T} \approx 1 - \beta\Delta E$. The maximal negative Hall conductivity mainly dominated by the gapped DT in the lowest triplon bands is $\kappa_N^{xy} \approx P_t \Omega^{xy}(0) S_\Gamma$, where $\Omega^{xy}(0) S_\Gamma$ gives the $-\pi$ flux. Thus we have $\kappa_N^{xy} \approx -\pi(1 - \beta J + 2\beta D'_{\perp})$. With increasing the $D'_{\perp}(\tilde{D}'_{\parallel})$, the maximal negative Hall conductivity also follows the linear relation.

Selective triplon density amplification by a driving field is another way to enhance thermal Hall signal without altering the nature of the ground state or the topological character of the magnon bands [30]. With a coherent driving electromagnetic (EM) field, the anomalous triplon pairing terms can be created. The triplon density is determined by the time-dependent equation of motion as follows [30]:

$$i\frac{dT_k(t)}{dt} = \tilde{\Omega}_k T_k(t), \tag{9}$$

where $T_k(t) = (\langle t_k \rangle, \langle t^{\dagger}_{-k} \rangle)$ are the classical amplitudes of the triplon fields, and $\tilde{\Omega}_k$ is the dynamical matrix, which has the eigenvalues:

$$\omega_{k,\pm} = \frac{\omega_k - \omega_{-k}}{2} - \frac{i\gamma}{2} \pm \sqrt{\frac{(\omega_k + \omega_{-k} - \Omega_0)^2}{2} - \epsilon^2}, \tag{10}$$

where γ gives the dissipative damping, and ϵ is the overall coupling strength. When the detuning term $\omega_k + \omega_{-k} - \Omega_0 \approx 0$, the imaginary part of $\omega_{k,+}$ becomes $\epsilon - \gamma/2$, and the triplon density at k is $\langle t_k \rangle \propto e^{(\epsilon - \gamma/2)t}$. When the coupling strength ϵ exceeds the dissipation γ, there is an exponential growth of the triplon density of mode k, thus the resonant amplification is achieved. Due to the linear band dispersions $\omega = \omega_\Gamma + v_\Gamma k + O(k^2)$ with slope v_Γ of DT, the momentum and energy matching is easily fulfilled. We can estimate the resonant driving frequency $\Omega_0 = 2\omega_\Gamma$ around the DT only with the linear dispersion. We use the exchange parameter $J = 722$ GHz in $SrCu_2(BO_3)_2$ system, and it gives rise to the resonant frequency $\Omega_0 = 1.34$ THz. The linear-dispersive triplon at the M point has a relatively higher energy level, which requires a higher resonant frequency of about 1.44 THz to achieve the amplification. Thus, one can realize the triplon density amplification at selected momenta by choosing the driving light with different frequencies. It is also possible to achieve directional tunability of thermal Hall flow by precisely controlling the EM field at different k points, as shown in the schematic plot Fig. 4(b).

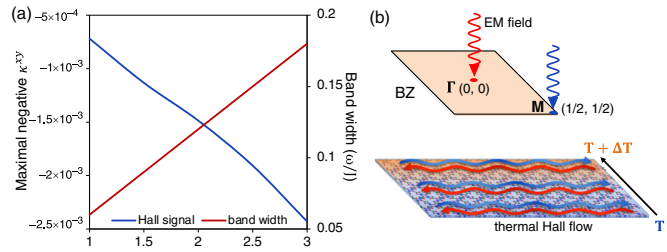

FIG. 4. (a) Enhancement of Hall signal by changing strength DM interactions. The x axis is the strength of DM term from $D'_{\perp}$ to $3D'_{\perp}$. Both bandwidth and maximal negative Hall signals are plot. (b) The schematic plot of triplon density amplification by external electromagnetic field at different k points, which shows the direction-tunable features of the thermal Hall flow.

Conclusions. To summarize, we found that the in-plane magnetic field (h_x) gives rise to a new type of Dirac point in the lowest bands at the BZ center (momentum $k = 0$) of the SSM, which has a π Berry flux nature. The induced negative thermal Hall conductance shows the possibility of the tunable

nontrivial thermal transport. We also show that the negative thermal Hall conductance can be potentially enhanced by increasing the DM interaction and using an EM field-driven amplification. Based on the TB model, we develop an effective low-energy model showing that h_x induces a Rashba-like SOC, leading to useful insight into the bosonic Rashba SOC physics. One can possibly detect this SOC induced pseudospin texture distributions in momentum space. It is also worth noting that the tilted magnetic field induces flat lowest bands. Once these interaction effects are added, bosonic systems hold the promise of realizing new interaction-driven topological phases, where magnetic-induced flat triplon bands are ideally suited for realizing the complex bosonic phases in a controllable manner.

Acknowledgments. Y.B. would like to acknowledge the support by the National Research Foundation, Singapore under the NRF fellowship award (NRF-NRFF12-2020-005). S.H. and D.N. would like to acknowledge the support by Ministry of Education, Singapore, under Grant No. AcRF TIER 1 2019-T1-002-050 (RG 148/19 (S)). P.S. acknowledges financial support from the Ministry of Education, Singapore through MOE2018-T1-001-021.

[1] B. Shastry and B. Sutherland, Physica B+C **108**, 1069 (1981).
[2] S. Miyahara and K. Ueda, Phys. Rev. Lett. **82**, 3701 (1999).
[3] K. Kodama, M. Takigawa, M. Horvatić, C. Berthier, H. Kageyama, Y. Ueda, S. Miyahara, F. Becca, and F. Mila, Science **298**, 395 (2002).
[4] S. E. Sebastian, N. Harrison, P. Sengupta, C. D. Batista, S. Francoual, E. Palm, T. Murphy, N. Marcano, H. A. Dabkowska, and B. D. Gaulin, Proc. Natl. Acad. Sci. USA **105**, 20157 (2008).
[5] M. Jaime, R. Daou, S. A. Crooker, F. Weickert, A. Uchida, A. E. Feiguin, C. D. Batista, H. A. Dabkowska, and B. D. Gaulin, Proc. Natl. Acad. Sci. USA **109**, 12404 (2012).
[6] G. Radtke, A. Saúl, H. A. Dabkowska, M. B. Salamon, and M. Jaime, Proc. Natl. Acad. Sci. USA **112**, 1971 (2015).
[7] P. A. McClarty, F. Krüger, T. Guidi, S. F. Parker, K. Refson, A. W. Parker, D. Prabhakaran, and R. Coldea, Nat. Phys. **13**, 736 (2017).
[8] M. E. Zayed, C. Rüegg, J. Larrea J., A. M. Läuchli, C. Panagopoulos, S. S. Saxena, M. Ellerby, D. F. McMorrow, T. Strässle, S. Klotz, G. Hamel, R. A. Sadykov, V. Pomjakushin, M. Boehm, M. Jiménez-Ruiz, A. Schneidewind, E. Pomjakushina, M. Stingaciu, K. Conder, and H. M. Rønnow, Nat. Phys. **13**, 962 (2017).
[9] B. D. Gaulin, Nat. Mater. **4**, 269 (2005).
[10] K.-K. Ng and T. K. Lee, Phys. Rev. Lett. **97**, 127204 (2006).
[11] P. Sengupta and C. D. Batista, Phys. Rev. Lett. **98**, 227201 (2007).
[12] P. Sengupta and C. D. Batista, Phys. Rev. Lett. **99**, 217205 (2007).
[13] L. Balents, Nature (London) **464**, 199 (2010).
[14] P. Chen, C.-Y. Lai, and M.-F. Yang, Phys. Rev. B **81**, 020409(R) (2010).
[15] Y. F. Cheng, O. Cépas, P. W. Leung, and T. Ziman, Phys. Rev. B **75**, 144422 (2007).
[16] J. Romhányi, K. Penc, and R. Ganesh, Nat. Commun. **6**, 6805 (2015).
[17] H. Kageyama, K. Yoshimura, R. Stern, N. V. Mushnikov, K. Onizuka, M. Kato, K. Kosuge, C. P. Slichter, T. Goto, and Y. Ueda, Phys. Rev. Lett. **82**, 3168 (1999).
[18] C. Knetter, A. Bühler, E. Müller-Hartmann, and G. S. Uhrig, Phys. Rev. Lett. **85**, 3958 (2000).
[19] Z. Wang and C. D. Batista, Phys. Rev. Lett. **120**, 247201 (2018).
[20] S. Raghu and F. D. M. Haldane, Phys. Rev. A **78**, 033834 (2008).
[21] H. Katsura, N. Nagaosa, and P. A. Lee, Phys. Rev. Lett. **104**, 066403 (2010).
[22] L. Zhang, J. Ren, J.-S. Wang, and B. Li, Phys. Rev. Lett. **105**, 225901 (2010).
[23] K. A. van Hoogdalem, Y. Tserkovnyak, and D. Loss, Phys. Rev. B **87**, 024402 (2013).
[24] K. F. Mak, D. Xiao, and J. Shan, Nat. Photonics **12**, 451 (2018).
[25] Z.-F. Xu, L. You, A. Hemmerich, and W. V. Liu, Phys. Rev. Lett. **117**, 085301 (2016).
[26] See Supplemental Material http://link.aps.org/supplemental/10.1103/PhysRevB.103.L140404 for more information.
[27] D. Bercioux and P. Lucignano, Rep. Prog. Phys. **78**, 106001 (2015).
[28] A. Manchon, H. C. Koo, J. Nitta, S. M. Frolov, and R. A. Duine, Nat. Mater. **14**, 871 (2015).
[29] R. Matsumoto and S. Murakami, Phys. Rev. Lett. **106**, 197202 (2011).
[30] D. Malz, J. Knolle, and A. Nunnenkamp, Nat. Commun. **10**, 3937 (2019).